WOOD RESEARCH **doi.org/10.37763/wr.1336-4561/71.4.584596**
e-ISSN 2729-8906
71(4): 2026 584-596 pp.

EXPERIMENTAL ASSESSMENT OF REINFORCEMENT ANCHORAGE IN CLT GROOVES UNDER TENSILE LOADING

KLARA FREUDENBERGER, TOMÁŠ KLAS, JÁN BRODNIANSKY,
JAROSLAV SANDANUS, MARTIN MAGURA
SLOVAK UNIVERSITY OF TECHNOLOGY IN BRATISLAVA
SLOVAK REPUBLIC

RECEIVED OCTOBER 2026

ABSTRACT

Sixteen tensile tests examine reinforcement anchorage in cross-laminated timber (CLT) grooves for hybrid-floor continuity connections. Two concrete-groove widths, two epoxy systems and headed-bar pockets with and without screws are compared using peak forces, apparent quasi-linear stiffnesses, force–elongation curves and observed damage. Companion bar tests provide reference forces. Concrete grooves with basic widths of 45 and 55 mm reached mean peak forces of 24.80 and 21.71 kN, respectively, with continued force transfer after cracking. Mean peak forces were 46.71 kN for XEPOX FLUID and 51.89 kN for HIT–RE 500 V4. The Hilti specimens showed plastic deformation of the reinforcement, whereas the XEPOX curves formed two response groups. Two screws increased the headed-pocket peak force from 26.08 to 41.50 kN and altered cracking. HIT–RE 500 V4 and XEPOX FLUID exhibited mean apparent quasi-linear stiffnesses of 8.6 and 7.7 kN/mm, respectively.

KEYWORDS: Cross-laminated timber, reinforcement anchorage, quasi-linear stiffness, epoxy adhesive, concrete-filled groove.

INTRODUCTION

Connections between cross-laminated timber (CLT) panels and steel beams govern how forces are transferred through a hybrid floor. In a slim-floor arrangement, panels rest on the lower flange of a steel beam, while reinforcement near the upper surface can connect adjacent panels across the support. Anchoring this reinforcement in the timber panel is essential to developing the tensile force associated with continuity. The local anchorage therefore deserves separate examination before its behaviour is combined with panel bending and bearing at the support. CLT provides a layered substrate whose orientation and geometry must be considered in connection detailing (Brandner et al. 2016). Research on timber–concrete floors has similarly established the importance of connection behaviour to composite action (Yeoh et al. 2011). The study of panel connections in a hybrid slim-floor structure by Freudenberger (2023) provides the structural context for the anchorage details examined here.

Grooved timber–concrete connections transfer forces through bearing and geometric

interlock (Kanócz et al. 2014), whereas bonded systems use an adhesive interface (Kanócz and Bajzecerová 2015). Jiang and Crocetti (2019) examined notched CLT–concrete connections, while Mai et al. (2018) studied mechanical shear connectors with different inclinations. Hassanieh et al. (2016) characterised steel–CLT connections using push-out tests with bolts, screws and combined adhesive–screw connections. Numerical work on bonded steel connectors for point-supported CLT slabs provides a further example of local force transfer in hybrid details (Kázsmér and Sandanus 2026).

Glued-in rod research identifies the interaction of steel, adhesive and timber as central to anchorage performance (Tlustochowicz et al. 2011; Steiger et al. 2015). Pull-out studies address adhesive properties and bondline geometry (Broughton and Hutchinson 2001), anchorage length and rod diameter (Steiger et al. 2007; Rossignon and Espion 2008), and bondline fracture behaviour (Serrano 2001). Duchoň et al. (2016) investigated axial pull-out behaviour and timber beam joints with glued-in rods in bending. Shekhorkina et al. (2019) examined the load–slip response of dowel connections with slotted-in steel plates in glued timber under tension parallel to the grain. In CLT, experiments have examined rod orientation and layer-related failure (Azinović et al. 2018; Ayansola et al. 2022; Shirmohammadli et al. 2024), while numerical and experimental studies consider both capacity and stiffness (Azinović et al. 2019; Ling et al. 2025). These studies provide context for examining open grooves under tensile loading.

This study compares three reinforcement anchorage strategies for CLT panel connections: keyed concrete-filled grooves, epoxy-filled grooves and concrete pockets with headed bars. The comparison addresses concrete-groove width, the response of two epoxy systems and the addition of screws around the headed pocket. Peak forces, quasi-linear stiffness and observed damage are evaluated alongside companion reinforcement test results to compare the configurations. The sixteen component tests originate from Freudenberger (2024). The eight epoxy tests were previously reported by Freudenberger and Klas (2024); the present assessment combines these records with the concrete-groove and headed-pocket results and adds a consistent comparison of quasi-linear stiffness.

MATERIAL AND METHODS

Experimental programme

The programme comprised two concrete-groove series, two epoxy-groove series and a pair of headed-bar pockets (Tab. 1). Each specimen contained one 10 mm diameter B500B reinforcing bar. The concrete and epoxy specimens were cut from five-layer CLT into blocks measuring 375 × 150 × 200 mm. The headed-pocket blocks measured 250 × 250 × 200 mm.

Tab. 1: Test matrix and principal variables.

Configuration	Specimen identifiers	Number
Concrete, 45 mm basic width	1P45, 2P45, 3P45	3
Concrete, 55 mm basic width	4P, 5P, 6P	3
XEPOX FLUID	2RF1–2RF4	4
HIT–RE 500 V4	H1–H4	4
PSB without screws	PSB-0	1
PSB with two screws	PSB-2	1

Materials and loading arrangement

The Stora Enso CLT was manufactured from C24 timber, with the lamella orientation and groove direction corresponding to those of the intended floor connection. Concrete was specified as C16/20. The measured cube compressive strengths were 16.99 MPa for the straight-groove batch and 20.91 MPa for the headed-pocket batch. Two companion tensile tests characterised each reinforcement group (Tab. 2). Specimens were prepared successively in the laboratory at approximately the same ambient temperature. CLT moisture was 10.2% ± 1%.

Tab. 2: Companion reinforcement tensile tests; all bars were B500B, diameter 10 mm.

Associated specimens	**Test 1 (kN)**	**Test 2 (kN)**	**Mean (kN)**
Concrete and XEPOX series	51.88	53.20	52.54
HIT–RE 500 V4 series	54.77	55.80	55.29
Both PSB pockets	53.65	52.79	53.22

A steel reaction fixture was used in the Testometric FS500CT universal testing machine (Fig. 1). It supported the end face of the CLT block while keeping the groove infill clear of the support. The projecting reinforcement was held in the machine jaws and loaded in tension until failure of the specimen. This arrangement transferred the applied bar force into the CLT through the anchorage region, without direct bearing of the groove infill against the reaction fixture.

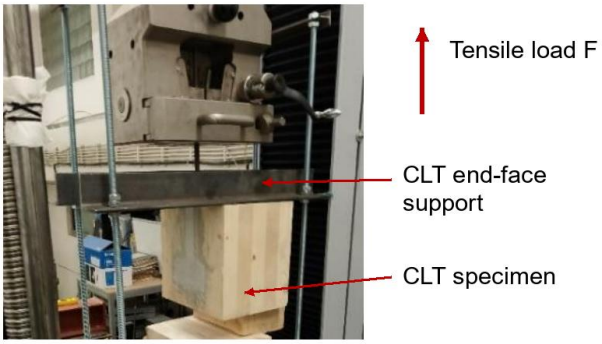


Fig. 1: Detail of the reaction fixture and specimen. The timber end face bears against the fixture while the groove infill remains clear of the support.

Concrete-filled grooves

The concrete grooves were 335 mm long and 53 mm deep, with local enlargements forming keys (Fig. 2). The basic width was 45 or 55 mm, and the reinforcement was positioned 20 mm above the groove bottom. The widths were selected to allow complete concrete filling around the bar. The reinforcement was secured during casting to maintain its position. The two series retained the same groove length, depth and key arrangement. A representative prepared specimen is shown in Fig. 2b.

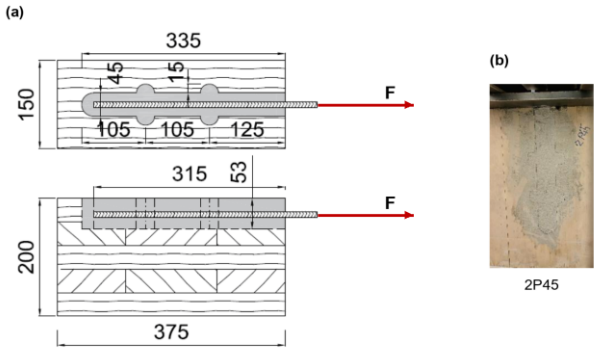


Fig. 2: Concrete-filled groove: (a) geometry of the 45 mm series with the tensile force F indicated; (b) representative specimen before testing. Dimensions in mm.

Epoxy-filled grooves

The epoxy grooves were 328 mm long, 16 mm wide and 40 mm deep (Fig. 3a). The groove depth accommodated the reinforcement position and the additional opening in the DELTABEAM used in subsequent tests. Four specimens contained Rothoblaas XEPOX FLUID, and four contained Hilti HIT–RE 500 V4. The groove ends were sealed before filling. The liquid XEPOX mixture required careful sealing, whereas the Hilti injection mortar had a thicker consistency. For XEPOX, the recommended clearance between the reinforcement and the timber was 2–3 mm. The reinforcement was positioned 10 mm above the groove bottom to suit the subsequent DELTABEAM tests. For Hilti, the recommended groove width was the reinforcement diameter plus 5.5 mm; the actual width exceeded this value by 0.5 mm. The reinforcement was positioned 7 mm above the groove bottom. These deviations from the recommended geometry accommodated the connection to the DELTABEAM. The bar was positioned before the adhesive was applied. Fig. 3b shows representative specimens of both series: the XEPOX infill is cream coloured, whereas the Hilti mortar is red. Both series were tested in the reaction arrangement shown in Fig. 1 as infills for the groove connection.

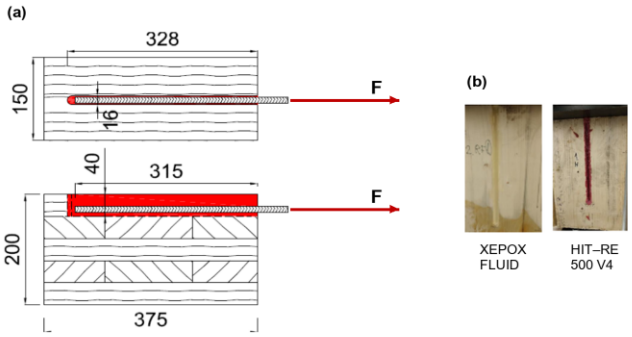


Fig. 3: Epoxy-filled groove: (a) geometry with the tensile force F indicated, dimensions in mm; (b) XEPOX FLUID specimen (left) and HIT–RE 500 V4 specimen (right) before testing.

Concrete pockets with headed reinforcement

The headed-bar configuration used a Peikko PSB bar in a locally widened concrete pocket (Fig. 4a). The axis of the bar was 25 mm above the groove bottom. The head introduced a bearing force into the concrete in the wider portion of the pocket. Specimen PSB-0 contained the headed bar alone; PSB-2 also contained two washer-head screws of 8 mm x100 mm.

The screws were partially driven into the timber, approximately midway along the lines joining the bar head to the rounded pocket edges, corresponding to a 45° breakout cone. Their intended role was to improve force transfer from the concrete pocket into the surrounding timber. Fig. 4b shows the specimens before casting. After these photographs were taken, the reinforcement was moved deeper into the pocket before casting. The CLT face was supported during loading while the concrete pocket remained clear of the reaction fixture.

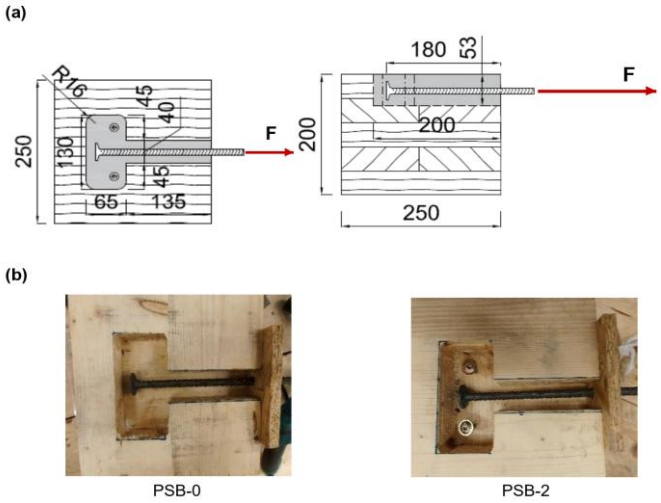


Fig. 4: Headed-bar pockets: (a) geometry with the tensile force F indicated, dimensions in mm; (b) specimens before casting, without screws (left) and with two screws (right). The bar was subsequently lowered to the final position specified in the text.

Evaluation of results

Peak forces were summarised by arithmetic means, sample standard deviations and coefficients of variation (CV). Force ratios express the mean peak force of each series, or the individual PSB peak force, relative to the associated mean companion-bar force (Tab. 2). Each PSB configuration is represented by one specimen. All calculations were performed before rounding. The apparent quasi-linear stiffness was evaluated as the secant slope:

$$K_{30-60} = \frac{\Delta F}{\Delta \delta} \quad (1)$$

$$\Delta F = 0.3\, F_{max} \quad (2)$$

$$\Delta \delta = \delta_{0.6} - \delta_{0.3} \quad (3)$$

where: $K_{30\text{-}60}$ – apparent quasi-linear stiffness, $\delta_{0.6}$ – elongation at 60% of F_{max} in the quasi-linear region of the measured curve, $\delta_{0.3}$ – elongation at 30% of F_{max} in the quasi-linear region of the measured curve.

Of the intervals examined, 30–60% of each specimen's peak force was the most suitable for consistent comparison across the measured curves in their quasi-linear region. The evaluation used the first loading branch of the experimentally measured force–elongation curves. The stiffness values describe the recorded assembly response. The specimen descriptions, measured forces, photographs and force–elongation curves originate from Freudenberger (2024); the descriptive statistics, force ratios and apparent stiffness comparison

are evaluated here.

RESULTS AND DISCUSSION

Peak forces and quasi-linear stiffness

Tab. 3 gives the peak forces, endpoint elongations and corresponding stiffnesses. The evaluated intervals are marked in Figs. 5, 7, 9 and 10.

Tab. 3: Peak forces and apparent quasi-linear stiffness of individual specimens.

Specimen	F_{max} (kN)	$\delta_{0.3}$ (mm)	$\delta_{0.6}$ (mm)	$\Delta\delta$ (mm)	K_{30-60} (kN/mm)
1P45	25.59	1.56	2.75	1.19	6.4
2P45	23.80	1.44	2.55	1.11	6.4
3P45	25.02	1.87	3.14	1.27	5.9
4P	18.96	2.99	3.94	0.95	6.0
5P	26.88	2.04	3.66	1.62	5.0
6P	19.28	1.84	3.07	1.23	4.7
2RF1	44.21	2.92	5.08	2.16	6.1
2RF2	43.18	3.61	5.49	1.88	6.9
2RF3	50.00	2.36	4.03	1.67	9.0
2RF4	49.43	2.71	4.38	1.67	8.9
H1	51.45	2.67	4.63	1.96	7.9
H2	52.27	4.90	6.86	1.96	8.0
H3	51.95	3.48	5.17	1.69	9.2
H4	51.87	2.67	4.36	1.69	9.2
PSB-0	26.08	3.13	4.66	1.53	5.1
PSB-2	41.50	2.62	4.66	2.04	6.1

$\delta_{0.3}$ and $\delta_{0.6}$: elongations at $0.30F_{max}$ and $0.60F_{max}$. Stiffness values are approximate; specimen configurations are listed in Tab. 1.

Concrete grooves with a basic width of 45 mm

The 45 mm series reached a mean peak force of 24.80 kN. The three peak forces were closely grouped (Fig. 5), with a CV of 3.69%. After the principal force drops, all three records show continued force transfer at lower levels as elongation increased.

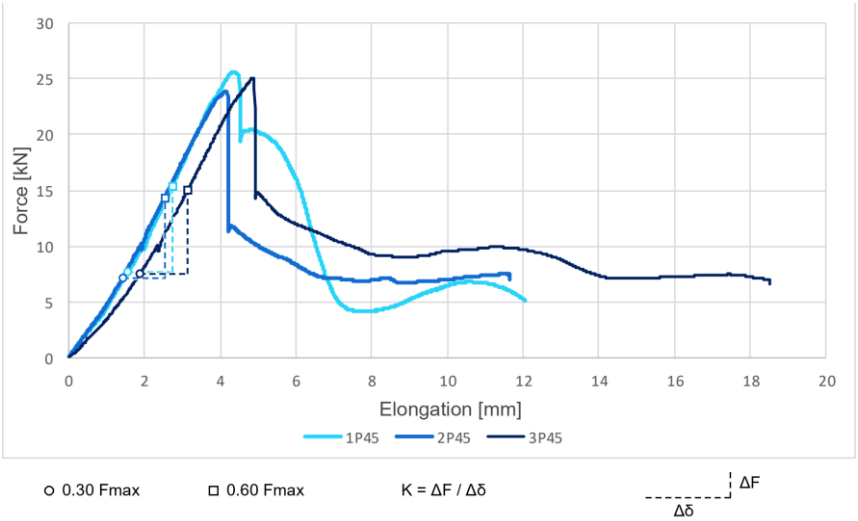


Fig. 5: Force–elongation curves for the 45 mm concrete grooves. Circles and squares mark 0.30Fmax and 0.60Fmax; dashed legs show Δδ and ΔF.

Specimen 1P45 developed a longitudinal crack along the groove. Specimen 2P45 developed a transverse crack at the first groove widening from the loaded end. The front concrete block was then withdrawn with the reinforcement, and a longitudinal crack developed. Specimen 3P45 showed a similar transverse crack, accompanied by a more pronounced longitudinal crack. The post-test views in Fig. 6 show how the damage followed the concrete-filled groove and its changes in width.

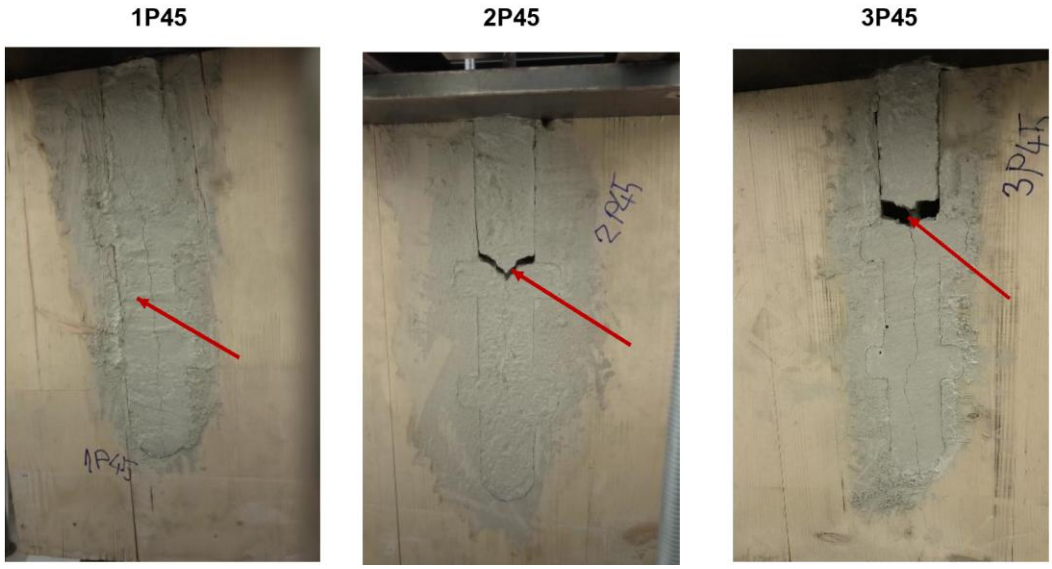


Fig. 6: Damage in the 45 mm concrete grooves after testing. Arrows identify a visible longitudinal crack in 1P45 and transverse cracks at groove widenings in 2P45 and 3P45. Specimen identifiers correspond to the curves in Fig. 5.

Concrete grooves with a basic width of 55 mm

The 55 mm series reached a mean peak force of 21.71 kN and showed greater scatter than the narrower series (CV 20.65%). Specimen 5P reached the highest individual force among all six concrete grooves, whereas 4P and 6P reached lower peaks (Fig. 7).

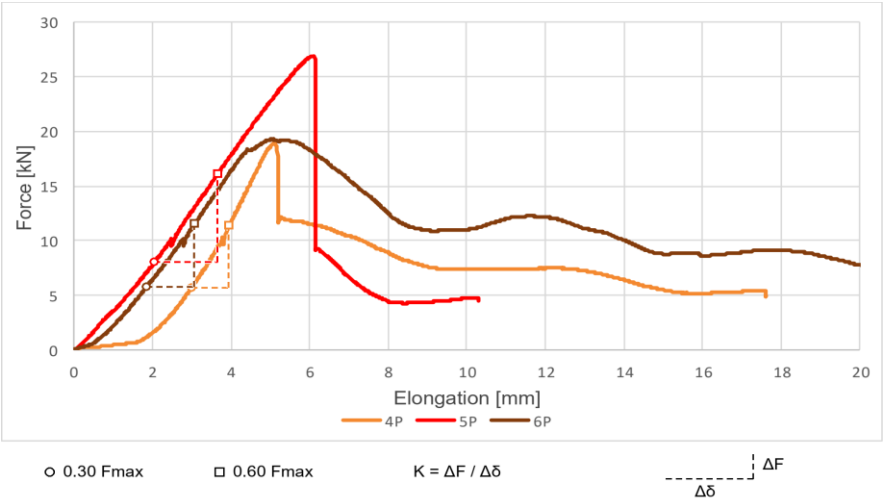


Fig. 7: Force–elongation curves for the 55 mm concrete grooves, with the stiffness evaluation intervals marked as in Fig. 5.

Specimen 4P developed a transverse crack at the first groove widening. In 5P, transverse cracking was accompanied by loss of bond between the reinforcing bar and the concrete in the rear part of the groove. In 6P, cracking at the first widening was followed by bar pull-out from the remaining rear concrete block. Fig. 8 shows the resulting damage and displacement of the concrete infill.

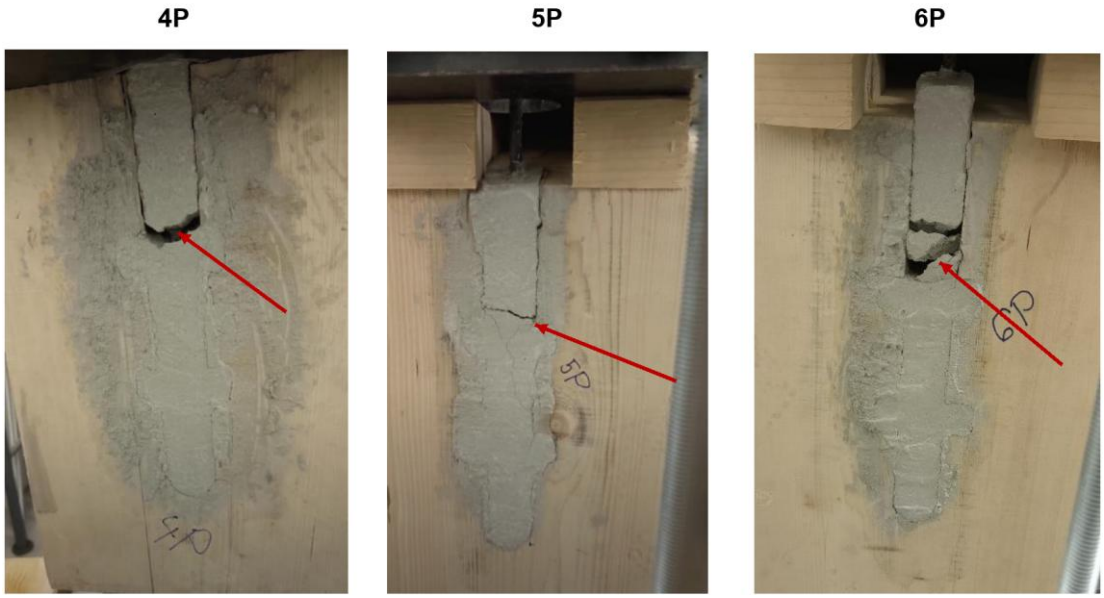
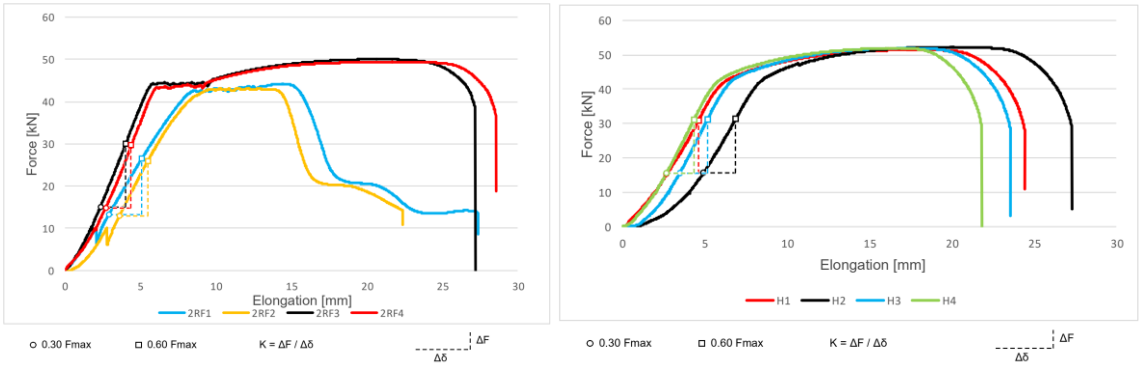


Fig. 8: Damage in the 55 mm concrete grooves after testing. Arrows identify visible transverse cracks and separated concrete regions in 4P, 5P and 6P. Specimen identifiers correspond to the curves in Fig. 7.

Epoxy-filled grooves

The XEPOX curves fall into two response groups (Fig. 9a). Specimens 2RF1 and 2RF2 show lower peak forces and descending residual-force branches, with bar pull-out following loss of the steel–epoxy bond. Specimens 2RF3 and 2RF4 show broad upper branches near the peak force, followed by abrupt terminal force drops. In these specimens, the reinforcement underwent plastic deformation, necking and rupture, without observed bond failure at either the steel–epoxy or epoxy–timber interface.



a) b)

Fig. 9: Force–elongation curves for (a) XEPOX FLUID and (b) HIT–RE 500 V4, with stiffness evaluation intervals marked as in Fig. 5.

The HIT–RE 500 V4 curves have closely grouped upper branches (Fig. 9b). Plastic deformation of the reinforcement was observed in all four specimens, without observed damage to the epoxy or material interfaces. The peak forces span 0.82 kN, and the series CV is 0.65%.

Headed reinforcement with and without screws

The PSB pocket without screws reached 26.08 kN, whereas the specimen with two screws reached 41.50 kN. The difference was 15.42 kN, corresponding to a 59.1% increase for this pair. Fig. 10 shows the higher peak force of the pocket with screws and the post-peak descending branches of both curves.

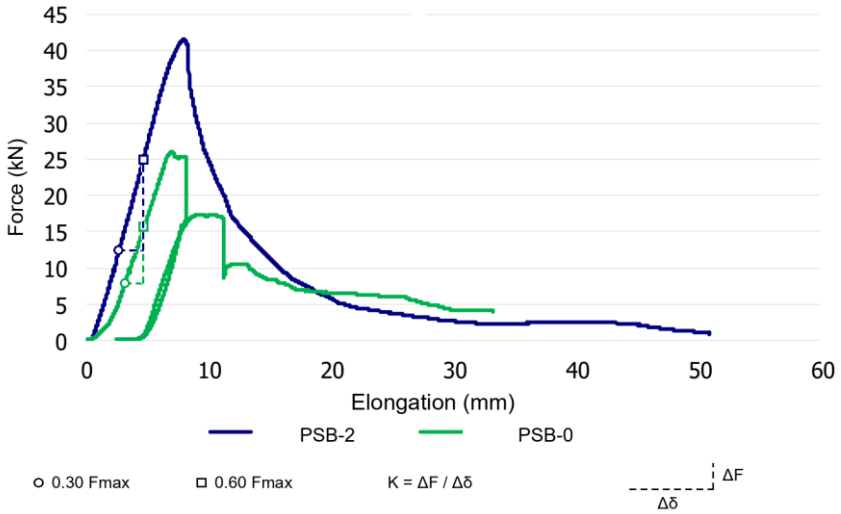


Fig. 10: Force–elongation curves for PSB-0 without screws and PSB-2 with two screws; stiffness evaluation intervals are marked as in Fig. 5.

The post-test photographs show concrete cracking around the headed region (Fig. 11). In the specimen without screws, inclined cracks extend from the central region towards the pocket sides. The specimen with screws exhibits a different crack pattern around the head and movement of the front concrete region. The observed damage is consistent with force transfer by head bearing into the concrete pocket and onward into the timber.

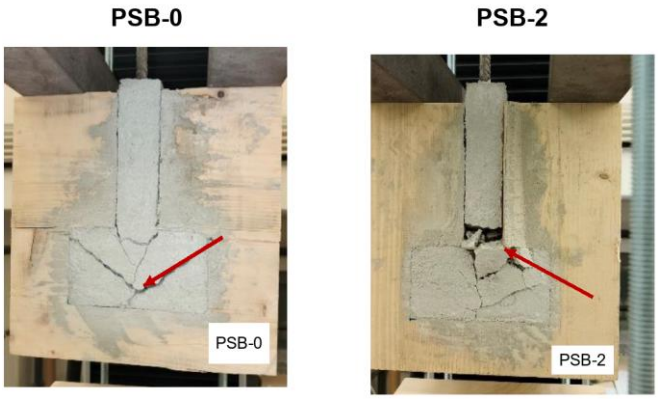


Fig. 11: Headed pockets after testing. Arrows identify visible cracks around the headed region in PSB-0 and PSB-2. The photographs document the different crack patterns associated with the responses in Fig. 10.

Comparison of forces and within-series scatter

Tab. 4 relates the anchorage peak forces to the corresponding companion-bar results. Normalisation helps distinguish differences in anchorage response from differences between the reinforcement groups.

Tab. 4: Descriptive statistics and comparison with companion reinforcement forces.

Configuration	n	Mean[1] (kN)	SD (kN)	CV (%)	Force ratio[2] (%)
Concrete 45 mm	3	24.80	0.91	3.69	47.2
Concrete 55 mm	3	21.71	4.48	20.65	41.3
XEPOX FLUID	4	46.71	3.51	7.51	88.9
HIT–RE 500 V4	4	51.89	0.34	0.65	93.9
PSB, no screws	1	26.08	—	—	49.0
PSB, two screws	1	41.50	—	—	78.0

[1]Individual measured force where n = 1. SD: sample standard deviation. [2] Mean or individual connection force divided by the mean of the associated companion bar tests. Ratios were calculated before rounding the bar means.

The Hilti mean peak force exceeded the XEPOX mean by 5.18 kN, but its companion-bar mean was also higher (55.285 versus 52.540 kN). Normalising by the respective bar means gives a difference of approximately 5.0 percentage points. The comparison therefore characterises each anchorage system in relation to its reinforcement group.

Concrete grooves and geometric interlock

Local enlargements provide bearing surfaces through which the concrete infill transfers force into the CLT. Transverse cracking at a key transition separates part of the infill and changes the effective anchorage region. The documented bar withdrawal and displaced concrete blocks are consistent with continued force transfer through the remaining rear region after the first major force drop. Increasing the base groove width from 45 to 55 mm did not result in a higher average maximum force in these tests. The average quasi-linear stiffness was also lower for the wider grooves: 5.2 versus 6.3 kN/mm. The wider series also exhibited greater scatter, although the 5P configuration achieved the highest individual force. Together with the formation of a crack at the point where the groove widens, these observations identify local geometry and the evolving concrete load-transfer zone as key aspects of the response. Concrete shear failure also governed the grooved timber–concrete shear specimens of Kanócz et al. (2014). This supports the importance of the concrete load-transfer region identified here, although the loading arrangements differ. The notched CLT–concrete connections examined by Jiang and Crocetti (2019) provide a further comparison for force transfer through local geometric interlock.

Epoxy grooves and bonded interfaces

The epoxy systems combined higher force transfer with a narrower infill region, consistent with the contribution of bonded interfaces in glued-in rod connections (Tlustochowicz et al. 2011; Duchoň et al. 2016). Mean stiffness was 8.6 kN/mm for HIT–RE 500 V4 (range 7.9–9.2) and 7.7 kN/mm for XEPOX FLUID (6.1–9.0). Within the XEPOX series, the higher stiffness of 2RF3 and 2RF4 coincided with reinforcement rupture, whereas 2RF1 and 2RF2 failed by pull-out. Azinović et al. (2018) reported failure between CLT layers in glued-in rod tests. Duchoň et al. (2016) reported steel-rod rupture and timber shear damage in epoxy-bonded

connections in solid timber. Ling et al. (2025) found that rod diameter, embedment length and grain orientation affected pull-out behaviour in CLT, and evaluated withdrawal stiffness alongside resistance. Their results support considering both measures; direct numerical comparison also depends on specimen geometry and the displacement definition.

Headed pockets and screws

The increase in peak force with screws (59.1%) was substantially greater than the increase in quasi-linear stiffness (approximately 19%). In this pair, the screws therefore affected the ultimate response more strongly than the stiffness in the selected loading interval. Together with the different crack pattern in Fig. 11, this is consistent with the screws influencing damage development and ultimate force transfer through the pocket. Component behaviour informs the assessment of complete members, as illustrated by the connection and beam tests of Khorsandnia et al. (2012). Here, the anchorage results informed the choice of details for subsequent hybrid CLT–steel connection specimens (Freudenberger 2024).

CONCLUSIONS

The sixteen tensile tests support four conclusions for the configurations examined: *(1)* Widening the keyed concrete grooves from 45 to 55 mm did not improve the mean peak force or mean quasi-linear stiffness under the tested conditions. *(2)* Epoxy-filled grooves achieved the highest mean peak forces and stiffnesses. HIT–RE 500 V4 had the higher mean stiffness and narrower range, whereas XEPOX FLUID exhibited two response groups. *(3)* In the headed-pocket pair, adding two screws improved both peak force and quasi-linear stiffness, with a larger relative gain in peak force. *(4)* Evaluation over 30–60% of peak force consistently distinguished anchorage stiffness within this test programme and complemented the comparison by peak force and observed damage.

ACKNOWLEDGMENTS

The preparation of this article was supported by the Scientific Grant Agency of the Ministry of Education, Research, Development and Youth of the Slovak Republic and the Slovak Academy of Sciences under project VEGA 1/0637/25.

REFERENCES

1. Ayansola, G.S., Tannert, T., Vallée, T., 2022: Experimental investigations of glued-in rod connections in CLT. Construction and Building Materials 324: 126680.
2. Azinović, B., Serrano, E., Kramar, M., Pazlar, T., 2018: Experimental investigation of the axial strength of glued-in rods in cross laminated timber. Materials and Structures 51(6): 143.
3. Azinović, B., Danielsson, H., Serrano, E., Kramar, M., 2019: Glued-in rods in cross laminated timber – Numerical simulations and parametric studies. Construction and Building Materials 212: 431–441.
4. Brandner, R., Flatscher, G., Ringhofer, A., Schickhofer, G., Thiel, A., 2016: Cross

laminated timber (CLT): overview and development. European Journal of Wood and Wood Products 74(3): 331–351.
5. Broughton, J.G., Hutchinson, A.R., 2001: Pull-out behaviour of steel rods bonded into timber. Materials and Structures 34(2): 100–109.
6. Duchoň, V., Klas, T., Katona, O., Brodniansky, J., Balcierák, Ľ., Sandanus, J., Sógel, K., 2016: Experimental tests of timber connections with glued-in rods in bending. Wood Research 61(4): 565–572.
7. Freudenberger, K., 2023: Analýza prepojenia panelov v hybridnej štíhlej stropnej konštrukcii (Analysis of the connection of panels in a hybrid slim ceiling structure). In: Advances in Architectural, Civil and Environmental Engineering. Spektrum STU, Bratislava, pp. 356–363 (in Slovak).
8. Freudenberger, K., 2024: Hybridné sústavy z ocele a CLT (Hybrid steel and CLT systems). Doctoral dissertation. Slovak University of Technology in Bratislava, Faculty of Civil Engineering, Bratislava. pp. 70–77, 80–100 (in Slovak).
9. Freudenberger, K., Klas, T., 2024: Connecting panels to steel beams: Results of tensile tests with epoxy adhesives. Stavebné materiály (6) (in Slovak).
10. Hassanieh, A., Valipour, H.R., Bradford, M.A., 2016: Load-slip behaviour of steel-cross laminated timber (CLT) composite connections. Journal of Constructional Steel Research 122: 110–121.
11. Jiang, Y., Crocetti, R., 2019: CLT-concrete composite floors with notched shear connectors. Construction and Building Materials 195: 127–139.
12. Kanócz, J., Bajzecerová, V., Šteller, Š., 2014: Timber–concrete composite elements with various composite connections. Part 2: Grooved connection. Wood Research 59(4): 627–638.
13. Kanócz, J., Bajzecerová, V., 2015: Timber–concrete composite elements with various composite connections. Part 3: Adhesive connection. Wood Research 60(6): 939–952.
14. Kázsmér, M., Sandanus, J., 2026: Innovative slab-column connector for a point-supported cross-laminated timber slabs in tall buildings – A numerical analysis. Slovak Journal of Civil Engineering 34(1): 21–36.
15. Khorsandnia, N., Valipour, H.R., Crews, K., 2012: Experimental and analytical investigation of short-term behaviour of LVL–concrete composite connections and beams. Construction and Building Materials 37: 229–238.
16. Ling, Z., Li, Z., Li, Z., Yang, C., Zheng, W., Zhang, L., 2025: Experimental investigation of axial pull-out behavior of glued-in threaded rods in cross-laminated timber. BioResources 20(3): 5407–5428.
17. Mai, K.Q., Park, A., Lee, K., 2018: Experimental and numerical performance of shear connections in CLT–concrete composite floor. Materials and Structures 51(4): 84.
18. Rossignon, A., Espion, B., 2008: Experimental assessment of the pull-out strength of single rods bonded in glulam parallel to the grain. Holz als Roh- und Werkstoff 66(6): 419–432.
19. Serrano, E., 2001: Glued-in rods for timber structures — a 3D model and finite element parameter studies. International Journal of Adhesion and Adhesives 21(2): 115–127.
20. Shekhorkina, S., Kesariisky, A., Makhinko, M., Nikiforova, T., Savytskyi, O., 2019: Experimental investigation and FEM modeling of glued timber connections with slotted-in steel plates. Slovak Journal of Civil Engineering 27(4): 18–23.

21. Shirmohammadli, Y., Hashemi, A., Masoudnia, R., Quenneville, P., 2024: Experimental investigation of cross-laminated timber connections with glued-in rods under monotonic and cyclic loading. Journal of Structural Engineering 150(4): 04024018.
22. Steiger, R., Gehri, E., Widmann, R., 2007: Pull-out strength of axially loaded steel rods bonded in glulam parallel to the grain. Materials and Structures 40(1): 69–78.
23. Steiger, R., Serrano, E., Stepinac, M., Rajčić, V., O'Neill, C., McPolin, D., Widmann, R., 2015: Strengthening of timber structures with glued-in rods. Construction and Building Materials 97: 90–105.
24. Tlustochowicz, G., Serrano, E., Steiger, R., 2011: State-of-the-art review on timber connections with glued-in steel rods. Materials and Structures 44(5): 997–1020.
25. Yeoh, D., Fragiacomo, M., De Franceschi, M., Koh, H.B., 2011: State of the art on timber-concrete composite structures: Literature review. Journal of Structural Engineering 137(10): 1085–1095.

KLARA FREUDENBERGER, TOMÁŠ KLAS*, JÁN BRODNIANSKY,
JAROSLAV SANDANUS, MARTIN MAGURA
SLOVAK UNIVERSITY OF TECHNOLOGY IN BRATISLAVA
FACULTY OF CIVIL ENGINEERING
RADLINSKÉHO 11, 810 05 BRATISLAVA
SLOVAK REPUBLIC
*Corresponding author: tomas.klas@stuba.sk